FIRST INTERNATIONAL MULTIPHASE FLUID TRANSIENTS SYMPOSIUM

edited by
H. H. SAFWAT
J. BRAUN
U. S. ROHATGI

FED-Vol. 41

FIRST INTERNATIONAL MULTIPHASE FLUID TRANSIENTS SYMPOSIUM

presented at

THE WINTER ANNUAL MEETING OF
THE AMERICAN SOCIETY OF MECHANICAL ENGINEERS
ANAHEIM, CALIFORNIA
DECEMBER 7–12, 1986

sponsored by

THE FLUID TRANSIENTS AND
MULTIPHASE FLOW COMMITTEES,
THE FLUIDS ENGINEERING DIVISION, ASME

edited by

H. H. SAFWAT
BECHTEL WESTERN POWER CORPORATION

J. BRAUN
UNIVERSITY OF AKRON

U. S. ROHATGI
BROOKHAVEN NATIONAL LABORATORY

THE AMERICAN SOCIETY OF MECHANICAL ENGINEERS
United Engineering Center 345 East 47th Street New York, N.Y. 10017

Library of Congress Catalog Card Number 86-72524

FOREWORD

This symposium has been organized and sponsored by the Fluid Transients and the Multiphase Flow Committees of the Fluids Engineering Division, ASME. The main purpose of the symposium is to focus attention on recent work in multiphase fluid transients covering one dimensional flow in pipes and multidimensional flows. The intent was to bring together experts working in these areas from around the world. The scope of the symposium covers both experimental and numerical aspects. Professor Sanjoy Banerjee's keynote speech entitled "Current Approaches to Modeling Multicomponent, Multiphase Flows, Problems, and Potential" gives a summary of status and projections for future work. (His contribution is not included in this volume.) The symposium papers cover a wide range of problems ranging from wave speed propagation in bubbly flow, oscillatory flow in air-water mixture, oscillatory flows in nozzles, slugging in refrigeration compressors, rapid condensation, flows in self actuating valves, transients in cooling water systems and multi-component flows through packed beds.

It is the objective of the symposium to create a forum for exchange of ideas, expose new techniques and methods. It is hoped that both the participants and the readers will benefit from this volume in the continuing endeavors to improve the understanding, of multiphase transient phenomena and enable development of improved analysis methods for the numerous problems that face the practicing engineers in the area of multiphase fluid transients.

Hemmat H. Safwat
Bechtel Western Power Corporation

Jack Braun
The University of Akron

Upendra S. Rohatgi
Brookhaven National Laboratory

CONTENTS

AN INVESTIGATION OF THE PROPAGATION OF PRESSURE PERTURBATIONS IN BUBBLY AIR/WATER FLOWS

A. E. Ruggles and H. A. Scarton
Department of Mechanical Engineering
Aeronautical Engineering and Mechanics

R. T. Lahey, Jr.
Department of Nuclear Engineering and Science
Rensselaer Polytechnic Institute
Troy, New York

ABSTRACT

Dispersion and attenuation was measured for standing waves in a vertical waveguide filled with a bubbly air/water mixture. The propagation speed of pressure pulses was also measured. The data was compared with a two-fluid model for a range of values of the virtual volume coefficient, C_{VM}. The C_{VM} representing the best fit to the data is given as a function of void fraction. The experimentally determined values of C_{VM} were found in general to be lower than those predicted by analytical models proposed by Zuber [2] and Van Wijngaarden [3].

NOMENCLATURE

a_{VM}	Virtual mass acceleration
B_ℓ	Coefficient of volumetric expansion for a liquid
$C_{2\phi}$	Speed of propagation of pressure perturbations in a two-phase mixture
C_{VM}	Virtual volume coefficient
c_p	Constant pressure specific heat capacity
c_v	Constant volume specific heat capacity
$\frac{D_g(\ )}{Dt}$	Material derivative, $\frac{\partial(\ )}{\partial t} + u_g \frac{\partial(\ )}{\partial z}$
f	Frequency
F	Force
g	Gravitational acceleration
H_{io}	Interfacial heat transfer coefficient
h	Enthalpy
i	Imaginary number, $\sqrt{-1}$
k	Wavenumber
$1/L_S$	Interfacial area density
p	Pressure
q''_{ki}	Interfacial heat transfer rate
R	Radius
T	Temperature
t	Time
u	Velocity
v	Specific volume
z	Axial location

Greek

α	Void fraction
η	Attenuation coefficient
λ	Wave length
μ	Dynamic viscosity
ω	Angular frequency
ρ	Density
σ	Surface tension
θ	Angle of inclination of flow from vertical

Subscripts

b	Bubble
2ϕ	Two-phase
g	Gas
i	Interfacial
ℓ	Liquid
0	Equilibrium value
VM	Virtual mass

Symbols

$\bar{(\ )}$	Effective value
$\langle\ \rangle$	Area averaging over the flow area
$\delta(\ )$	Perturbation
$(\ )^T$	Transpose of an array

INTRODUCTION

The virtual volume coefficient, C_{VM}, is important in the proper representation of interfacial momentum transfer in a two-fluid model of two-phase flow [1]. The functional relationship of the virtual volume coefficient to other pertinent flow characteristics such as global void fraction, $\langle\alpha\rangle$, and phase distribution has been the subject of prior research. Zuber [2] and Van Wijngaarden [3] have proposed theoretical models for the dependence of the virtual volume coefficient, C_{VM}, on global void fraction $\langle\alpha\rangle$, for bubbly flows:

$$C_{VM} = C_{VM_o}\left[\frac{1 + 2\langle\alpha\rangle}{1 - \langle\alpha\rangle}\right] \quad , \quad \text{(Zuber [1])} \qquad (1)$$

$$C_{VM} = C_{VM_o}\left[1 + 2.78\ \langle\alpha\rangle\right] \quad , \quad \text{(Van Wijngaarden [2])} \qquad (2)$$

where,

C_{VM_o} = 0.5, for a spherical bubble.

These models both predict increasing values of C_{VM} with increasing void fraction, $\langle\alpha\rangle$. Verification of this trend is given by data from various sources [4], [5], [6], and [7]. However, more definitive data is needed to establish a functional relationship between C_{VM} and $\langle\alpha\rangle$, in which careful control is exercised over all potentially important flow characteristics.

The purpose of the experimental study described herein was to obtain such data, and to establish an empirical relationship between the virtual volume coefficient and global void fraction in a dispersed bubbly air/water mixture. A correlation was derived by comparing sound propagation speeds and attenuations measured in a bubbly air/water mixture with those predicted using a two-fluid model[1] [8]. The two-fluid model used included models for the effects of bubble dynamics, viscous flow effects, and interfacial heat transfer [9]. The two-fluid model used in this study will now be summarized.

The gas continuity equation is

$$\rho_g \frac{\partial\alpha}{\partial t} + \alpha \frac{\partial p_g}{\partial t} + \rho_g u_g \frac{\partial\alpha}{\partial z} + \alpha\left[\rho_g \frac{\partial u_g}{\partial z} + u_g \frac{\partial p_g}{\partial z}\right] = 0, \qquad (3)$$

where for an ideal gas,

$$\frac{\partial p_g}{\partial t} = \frac{p_g}{P_g}\frac{\partial p_g}{\partial t} - \frac{\rho_g}{h_g}\frac{\partial h_g}{\partial t}$$

and,

$$\frac{\partial p_g}{\partial z} = \frac{p_g}{P_g}\frac{\partial p_g}{\partial z} - \frac{\rho_g}{h_g}\frac{\partial h_g}{\partial z} .$$

The liquid continuity equation is,

$$-\rho_\ell \frac{\partial\alpha}{\partial t} + (1 - \alpha)\left[\beta_\ell \frac{\partial p_\ell}{\partial t} + \phi_\ell \frac{\partial h_\ell}{\partial t}\right] - \rho_\ell u_\ell \frac{\partial\alpha}{\partial z}$$

$$+ (1 - \alpha)\left[u_\ell\beta_\ell \frac{\partial p_\ell}{\partial z} + u_\ell\phi_\ell \frac{\partial h_\ell}{\partial z} + \rho_\ell \frac{\partial u_\ell}{\partial z}\right] = 0 \qquad (4)$$

where,

$$\beta_\ell = \left.\frac{\partial\rho_\ell}{\partial p_\ell}\right|_{h_\ell}$$

and,

$$\phi_\ell = \left.\frac{\partial\rho_\ell}{\partial h_\ell}\right|_{p_\ell} .$$

The gas phase momentum equation is,

$$\rho_g\left[\frac{\partial u_g}{\partial t} + u_g\frac{\partial u_g}{\partial z}\right] + \frac{\partial p_g}{\partial z} - g\cos\theta\left[\frac{\rho_g}{p_g}p_g - \frac{\rho_g}{h_g}h_g\right]$$

$$+ F_D + F_{VM} + \delta F_R + \delta F_B = 0 \quad , \qquad (5)$$

and the liquid phase momentum equation is,

$$(1 - \alpha)\rho_\ell\left[\frac{\overline{\partial u_\ell}}{\partial t} + u_{\ell o}\frac{\overline{\partial u_\ell}}{\partial z}\right] + (1 - \alpha)\frac{\partial p_\ell}{\partial z}$$

$$+ \frac{\partial\alpha}{\partial z}(p_{\ell_i} - p_\ell) - (1 - \alpha)\, g\cos\theta\,(\rho_\ell)$$

$$- \alpha[F_D + F_{VM} + F_R + F_B] + F_W = 0 \qquad (6)$$

where,

F_D ≡ the drag force

$F_{VM} \triangleq \rho_\ell C_{VM} a_{VM}$ = virtual mass force

F_R ≡ radial reaction force due to bubble radius variations

F_B ≡ Basset force

F_W ≡ wall shear force

It is straightforward to show,

$$(p_{\ell_i} - p_\ell) = \rho_\ell\left[\overline{R_b\left(\frac{D^2R_b}{Dt^2}\right)} + \frac{3}{2}\overline{\left(\frac{DR_b}{Dt}\right)^2} - \frac{1}{4}\overline{(u_g - u_\ell)^2}\right] .$$

In this study the virtual mass acceleration, a_{VM}, was given by,

$$a_{VM} = \left|\frac{\overline{\partial u_g}}{\partial t} + u_g\frac{\overline{\partial u_g}}{\partial z}\right| - \left|\frac{\overline{\partial u_\ell}}{\partial t} + u_\ell\frac{\overline{\partial u_\ell}}{\partial z}\right| .$$

Since the purpose of this study was to investigate the propagation of pressure perturbations in air/water mixtures, the gas phase energy equation was not used in its normal form. Rather, the problem of the dynamics of an individual gas bubble in a liquid media was solved explicitly to relate the gas enthalpy and bubble radius to the liquid pressure and enthalpy. This analysis results in,

$$\frac{D^2R_b}{Dt^2} + 2\beta\frac{DR_b}{Dt} + \omega_n^2 R_b + \frac{p_\ell}{\rho_\ell R_b} = 0 \qquad (7)$$

where,

$$\beta = \beta_{VIS} + \beta_{TH} + \beta_{AC} + \beta_{COM} + \beta_{BL}$$

---

[1] The model presented in Ref. 8 was expanded during this effort. The thesis of Arthur E. Ruggles under the same title as this paper contains a description of the upgraded model. This thesis will be available in February of 1987.

and,

$$\omega_n^2 = \omega_{VIS}^2 + \omega_{TH}^2 + \omega_{AC}^2 + \omega^2{}_{COM} + \omega_{BL}^2 \ .$$

The terms contributing to the damping coefficient, β, and the resonant frequency, ω_n, are due to liquid viscosity (VIS), interfacial heat transfer (TH), acoustic scattering (AC), liquid compressibility (COM), and bulk liquid viscosity (BL), respectively [9].

Finally, the liquid phase thermal energy equation is given by,

$$(1-\alpha)\,\rho_\ell \left[\frac{\partial h_\ell}{\partial t} + u_\ell \frac{\partial h_\ell}{dz}\right] - (1-\alpha)\left[\frac{\partial p_\ell}{\partial t} + u_\ell \frac{\partial p_\ell}{dz}\right] - u_\ell F_w - \left[q''_{\ell_i}/L_s\right] = 0 \qquad (8)$$

where, $1/L_s$ is the interfacial area density.

Equations (3)-(8) can be written in matrix form as,

$$\underline{\underline{A}}\,\frac{\partial \underline{\psi}}{\partial t} + \underline{\underline{B}}\,\frac{\partial \underline{\psi}}{\partial z} = \underline{\underline{C}}\,\underline{\psi} \qquad (9)$$

where,

$$\underline{\psi} = \left[\alpha, p_\ell, u_g, u_\ell, h_\ell, R_b, \frac{D R_b}{Dt}\right]^T \qquad (10)$$

Equation (9) was perturbed as follows,

$$\left[\underline{\underline{A}}_o + \delta\underline{\underline{A}}\right]\left[\frac{\partial \delta\underline{\psi}}{\partial t}\right] + \left[\underline{\underline{B}}_o + \delta\underline{\underline{B}}\right]\left[\frac{\partial \underline{\psi}_o}{\partial z} + \frac{\partial \delta\underline{\psi}}{\partial z}\right] = \left[\underline{\underline{C}}_o + \delta\underline{\underline{C}}\right]\left[\underline{\psi}_o + \delta\underline{\psi}\right] \qquad (11)$$

The steady-state equation describing the unperturbed two-phase flow is given by,

$$\underline{\underline{B}}_o\,\frac{\partial \underline{\psi}_o}{\partial z} = \underline{\underline{C}}_o\underline{\psi}_o \qquad (12)$$

Assuming that the spatial derivatives of the steady-state solution are of order δ, the linearized equation set describing the response of the system to small perturbations is given by,

$$\underline{\underline{A}}_o\,\frac{\partial \delta\underline{\psi}}{\partial t} + \underline{\underline{B}}_o\,\frac{\partial \delta\underline{\psi}}{\partial z} = \underline{\underline{C}}'_o\,\delta\underline{\psi} \qquad (13)$$

where,

$$\underline{\underline{C}}'_o = \underline{\underline{C}}_o + \left.\frac{\partial \underline{\underline{C}}}{\partial \underline{\psi}}\right|_o \underline{\psi}_o$$

The perturbation of the state variables can be introduced in the form,

$$\delta\underline{\psi} = \underline{\psi}'\, e^{i(kz - \omega t)} \qquad (14)$$

Combining Eqs. (13) and (14) we obtain the algebraic equation,

$$\left\{\underline{\underline{A}}_o(\underline{\psi})\,[-i\omega] + \underline{\underline{B}}_o(\underline{\psi})\,[ik] - \underline{\underline{C}}'_o(\underline{\psi})\right\}\underline{\psi}' = 0 \ . \qquad (15)$$

Equation (15), in conjunction with the requirement that $\underline{\psi}'$ is finite, implies a dispersion relationship of the form,

$$\det\{(\omega\underline{\underline{A}}_o - i\underline{\underline{C}}'_o) - k\underline{\underline{B}}_o\} = 0 \ . \qquad (16)$$

For standing waves, Eq. (16) gives a relationship between real values of angular frequency, ω, and wavenumber, k. The wavenumber is in general a complex number with its real part corresponding to 2π divided by the wavelength and its imaginary part corresponding to an attenuation coefficient (η).

The propagation speeds and attenuation of pressure perturbations were measured for standing waves in a bubbly air/water flow with the global void fraction, $\langle\alpha\rangle$, varying from 0.5% to 18% and the bubble radii, R_b, varying from 0.5 mm to 2.5 mm. Frequencies were varied from 20 Hz to 200 Hz to allow measurement of the dispersion and attenuation curves for each flow situation. All standing wave measurements were taken with no liquid flow. The standing wave dispersion and attenuation data were compared with two-fluid model predictions for a range of values of the virtual volume coefficient. The value of C_{VM} giving the best agreement with a given data set was then chosen as the appropriate value.

Propagation speeds were also measured for pressure pulses. These measurements were performed for the same flow situations as the standing wave data, with the addition of varying the superficial liquid velocity from 0.0 m/sec to 1.0 m/sec. The pressure pulse propagation velocity data was compared with the nonlinear two-fluid model given by Eq. (9). To determine the pulse propagation speeds, the eigenvalues of the system were determined from,

$$\det\left[\underline{\underline{A}} - \xi\underline{\underline{B}}\right] = 0 \qquad (17a)$$

where,

$$\mathrm{Re}[\xi]_j = \left(\frac{dz}{dt}\right)_j^{-1} \qquad (17b)$$

Two of the eigenvalues of Eq. (17a) give the pulse propagation speed ($C_{2\phi}$). For example,

$$C_{2\phi} = \frac{\left|\left[\mathrm{Re}[\xi]_1\right]^{-1} - \left[\mathrm{Re}[\xi]_2\right]^{-1}\right|}{2} \ . \qquad (18)$$

The pressure pulse data was compared to the two fluid model using a range of values for C_{VM}. The value of C_{VM} producing the closest agreement with the data was chosen as the appropriate value for that flow situation.

STANDING WAVE MEASUREMENTS

The apparatus used for the standing wave measurements is shown in Figure 1. The waveguide used to generate the standing wave pattern was constructed from a 63.5 mm ID, 76.2 mm OD, stainless steel tube two meters in length. This tube was fitted with three side mounted pressure transducers and a hydrophone mounted on a traversing mechanism. Sinusoidal pressure oscillations were introduced through a side port, using an electromechanical shaker and piston arrangement. An isolation system prevented sound energy from the shaker and piston from entering the waveguide walls and disturbing the side mounted transducers. An air cushion isolated the entire wave guide and lower plenum from laboratory floor vibrations.

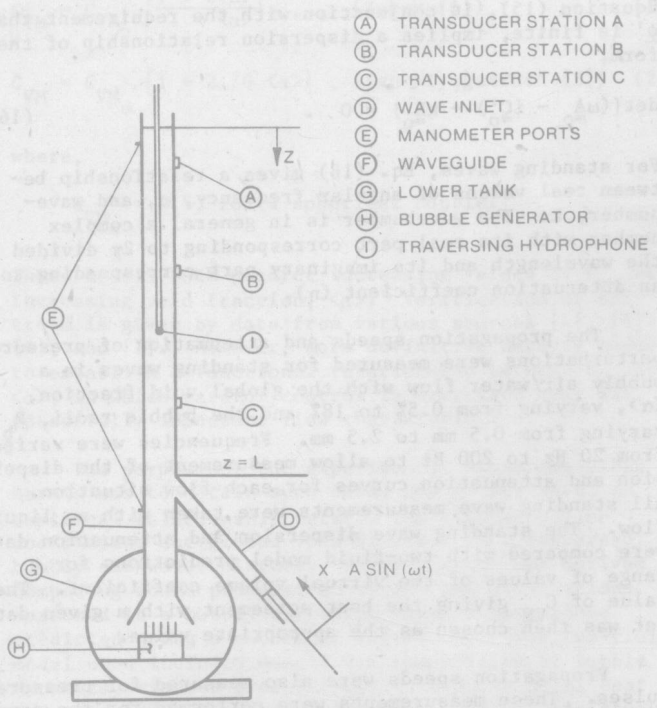

Figure 1: Measurement System for Sound Propagation in a Bubbly Air-Water Mixture.

Air bubbles were introduced in the lower plenum using one of four banks of hypodermic needles. The bubble radius produced by each needle was inferred through the measurement of the volume flow rate through the individual needles and measurement of the corresponding bubble departure frequency. Bubble radii were also measured directly using high speed photographic techniques. The distribution of bubble radii were measured for several flow rates for each bank. Figure 2 shows the bubble radii distributions of bank #3 for

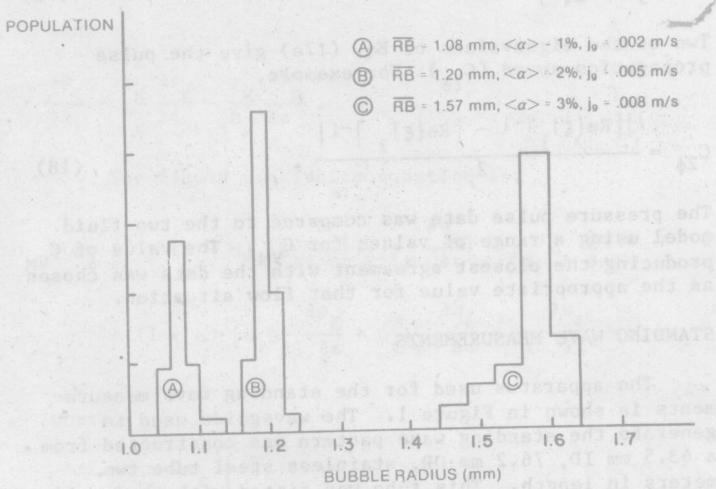

Figure 2: Bubble Radii Distributions, Bank 3 (Typical)

three different volumetric flow rates. Careful measurement of bubble radii is very important in low void fraction sound measurements because propagation speed is very sensitive to bubble radius when $\langle\alpha\rangle$ is less than 2%. The values of bubble radius for data taken in the region where $\langle\alpha\rangle$ is less than 7% were determined as des ribed above. In addition, subsequent experiments were performed using a clear acrylic section having quick closing valves. This section replaced the waveguide in the neighborhood of side-mounted transducer B. For runs having finite $\langle j_g \rangle$, the global void fraction was measured by simultaneously closing the quick closing valves. This avoided errors in trying to infer $\langle\alpha\rangle$ from measurements of the hydrostatic head. High speed photographs of the flow were also taken to allow the bubble size distribution to be determined. These observations accounted for any bubble coalescence that occured at the higher void fractions.

The propagation speed is also very sensitive to uncertainties in the measured void fraction. This is especially true for void fraction less than 3%. One of three manometers was used to measure the variation in hydrostatic pressure due to void fraction. The first of these measured global void fraction, $\langle\alpha\rangle$, from 0.000% to 1.000%, the second measured $\langle\alpha\rangle$ from 1.00% to 8.00%, and the third measured $\langle\alpha\rangle$ from 8.0% to 20.0 %. Three manometers were necessary to provide sufficient range and accuracy in the measurement of void fraction.

The propagation speed and attenuation of the pressure perturbations associated with standing waves was measured using three independent techniques. In the first of these techniques the hydrophone was traversed through the waveguide while the locations and amplitudes of the pressure nodes and anti-nodes were recorded. The propagation speed and attenuation could then be calculated since the distance between nodes is half of the wavelength, λ. That is,

$$C_{2\phi} = \lambda f \tag{19a}$$

$$\eta = \left(\frac{4\pi}{\lambda}\right) \sinh^{-1}\left\{\frac{|\delta p_{min}(n+1)| - |\delta p_{min}(n)|}{2|\delta p_{max}(n+\frac{1}{2})|}\right\} \tag{19b}$$

where, n is the node number, counting from the top of the wave guide.

The frequency, f, of the standing wave was measured using a Tektronix 7854 digital oscilloscope with a waveform calculator.

The second measurement technique used the root mean square pressure amplitude readings, δp_{RMS}, from the three side mounted transducers to infer the wavelength and attenuation of the standing wave. That is,

$$\frac{\delta p_{RMS}}{|A+|} = 2\, e^{-\eta \ell}\left[\cosh^2(\eta\ell) - \cosh^2\left(\frac{2\pi}{\lambda}\ell\right)\right]^{1/2}, \tag{20a}$$

where from Figure 1 the distance from the free surface is,

$$\ell = L - z \tag{20b}$$

and A+ is the amplitude of the upward traveling wave at z = L.

The third measurement technique involved varying the frequency until a pressure node was situated over one of the side mounted transducers. This indicated an integer number of half wave lengths existed between the transducer and the bubbly air/water interface with the ambient. The number of half wave lengths was then measured using the traversing hydrophone and the propagation speed was calculated using Eq. (19a). These

redundant measurement techniques were used to assure accuracy of the data and to verify that the presence of the traversing hydrophone did not affect the data.

An error analysis was performed using standard propagation of error techniques. The measurement uncertainties are given along with the standing wave data in Figures 3 through 12.

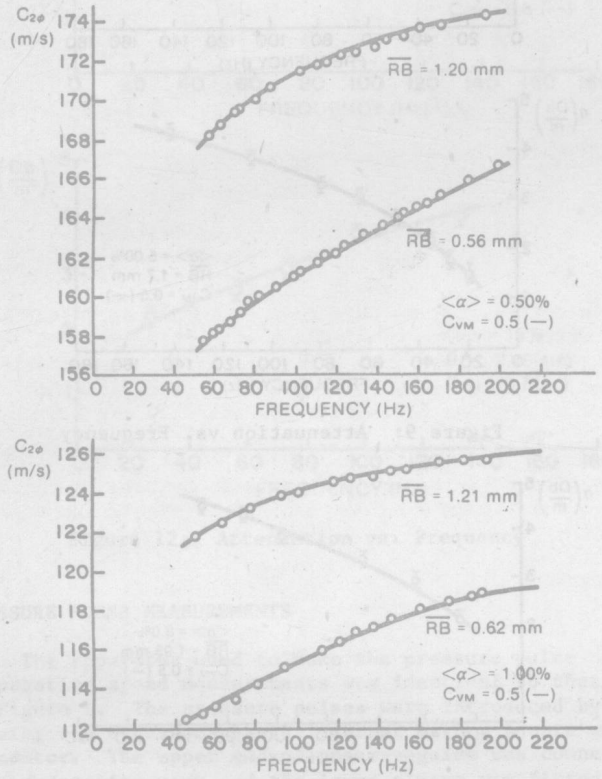

Figure 3: Propagation Speed vs. Frequency

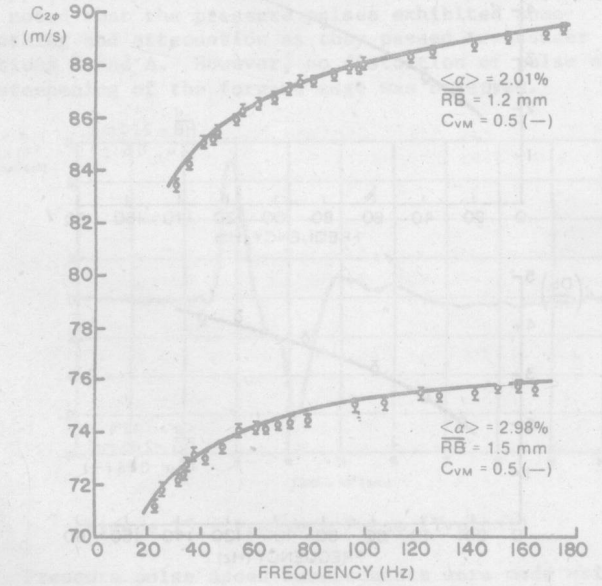

Figure 4: Propagation Speed vs. Frequency

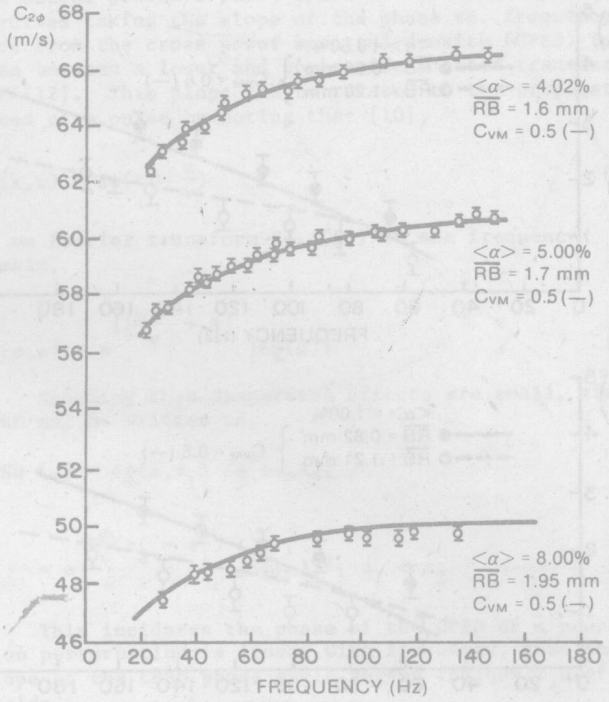

Figure 5: Propagation Speed vs. Frequency

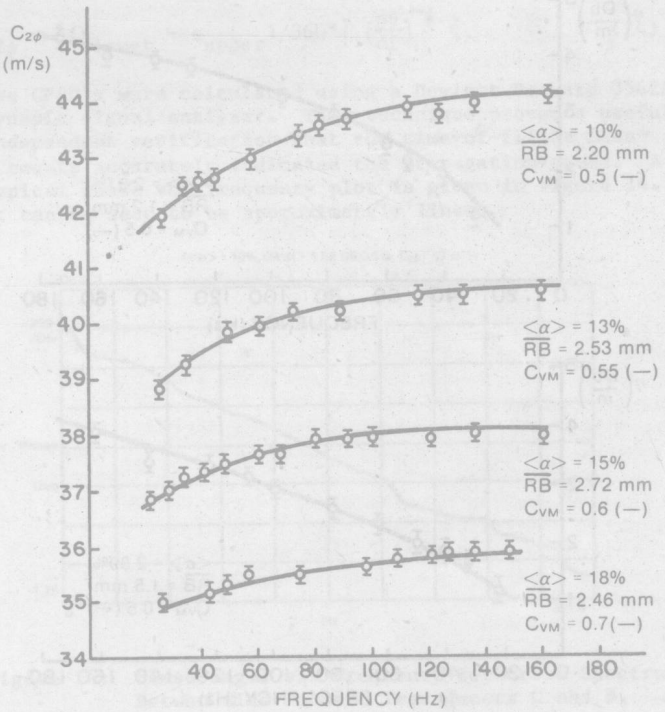

Figure 6: Propagation Speed vs. Frequency

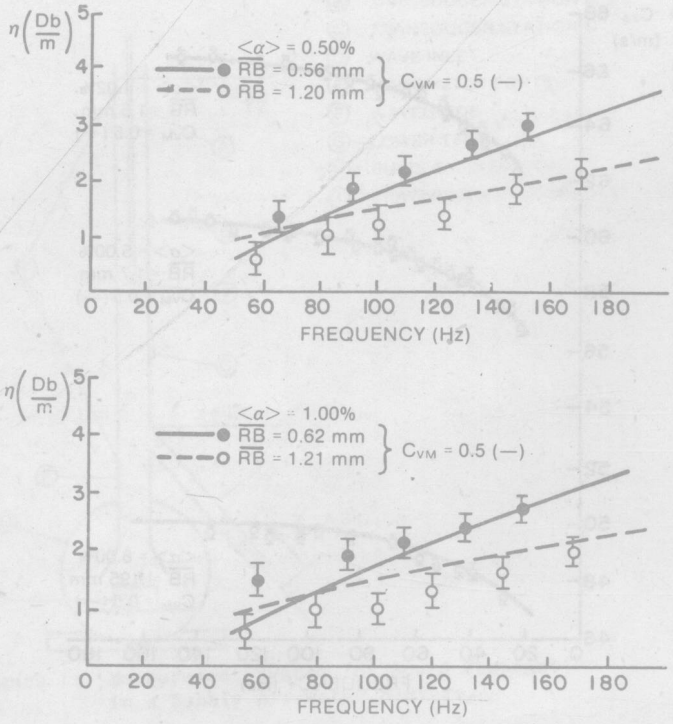

Figure 7: Attenuation vs. Frequency

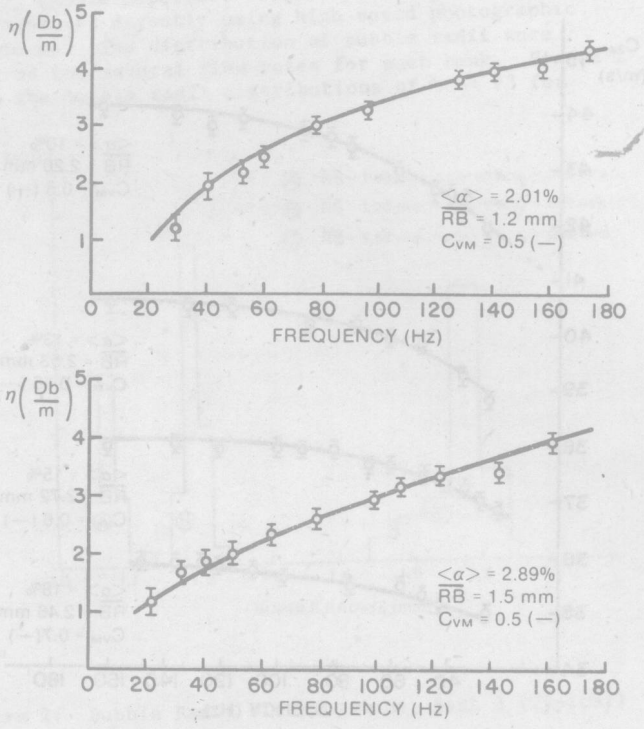

Figure 8: Attenuation vs. Frequency

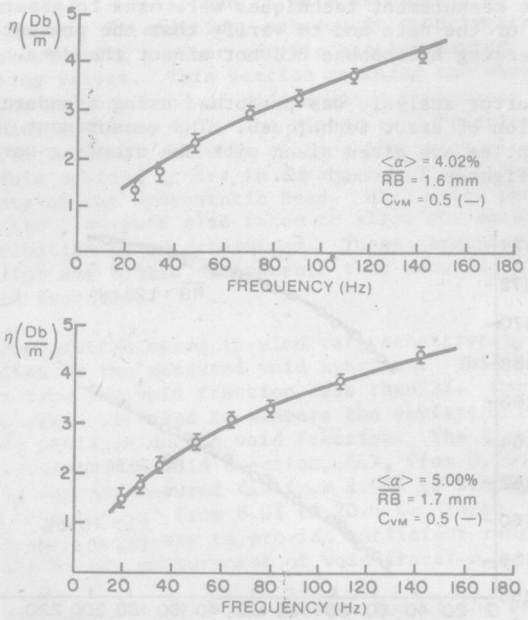

Figure 9: Attenuation vs. Frequency

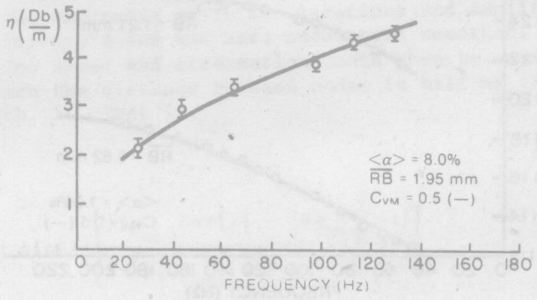

Figure 10: Attenuation vs. Frequency

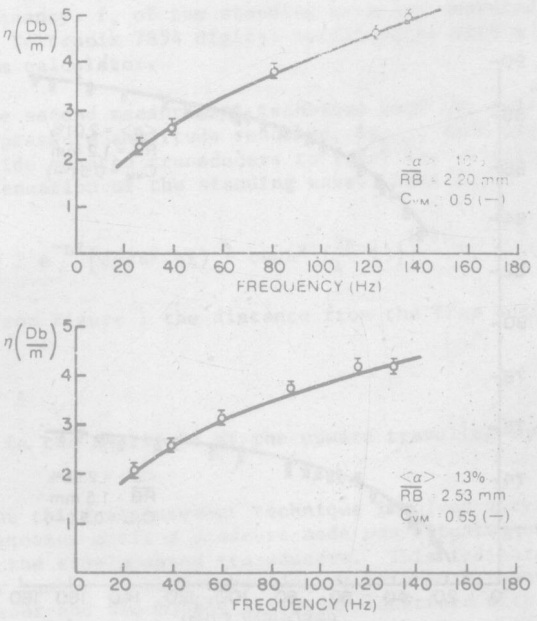

Figure 11: Attenuation vs. Frequency

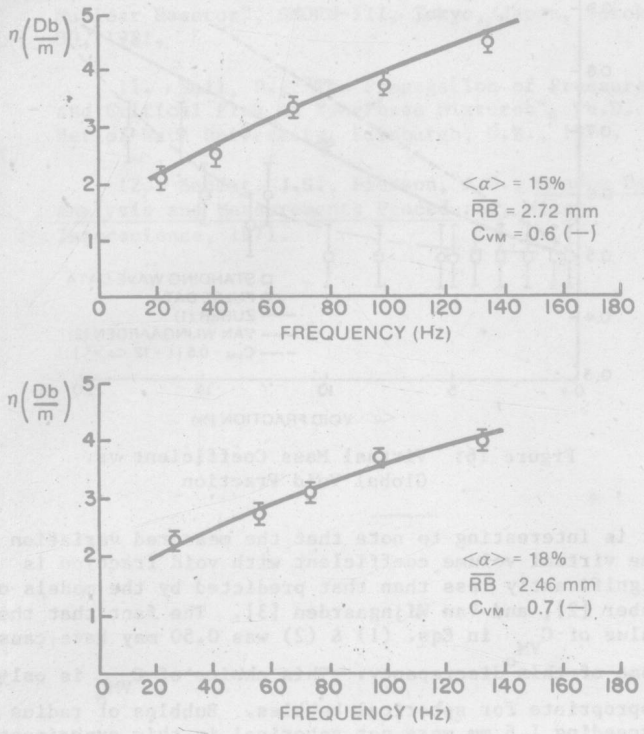

Figure 12: Attenuation vs. Frequency

PRESSURE PULSE MEASUREMENTS

The apparatus used to take the pressure pulse propagation speed measurements was identical to that in Figure 1. The pressure pulses were introduced by driving the electromechanical shaker with a square wave generator. The upper end of the waveguide was connected to a separation tank and the lower plenum was fitted with a metered water flow to facilitate variation of the superficial liquid velocity, $\langle j_\ell \rangle$.

A typical pressure pulse is given in Figure 13 as it appeared at transducer station C in Figure 1. It was noted that the pressure pulses exhibited some smoothing and attenuation as they passed transducer stations B and A. However, no distortion of pulse shape or steepening of the forward edge was observed.

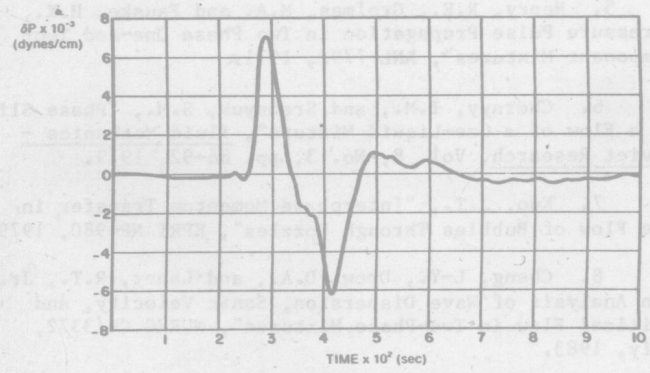

Figure 13: Pressure Pulse (Typical)

Pressure pulse speed measurements were made using two independent techniques. The first of these was a time-of-flight method. This technique used a Tektronix 7854 digital oscilloscope with the peak positive pressure chosen as the discrete time feature of each pulse. The second pressure pulse speed measurement technique involved taking the slope of the phase vs. frequency plot from the cross power spectral density (CPSD) function between a lower and upper side-mounted transducer set [12]. This slope can be related to the propagation speed of a pulse by noting that [10],

$$\delta\underline{\psi}(z,t) = \delta\underline{\psi}(t - \frac{z}{v}) \tag{21}$$

If we Fourier transform Eq. (21) to the frequency domain,

$$\delta\underline{\psi}(\omega,z) = e^{i\left[\frac{\omega z}{v} + \theta\right]} |\delta\underline{\psi}(\omega)| \tag{22}$$

Assuming that dispersion effects are small, the CPSD may be written as,

$$\text{CPSD}\ (\omega) = \delta\underline{\psi}(\omega,z_1)\ \delta\underline{\psi}^*(\omega,z_2)$$

$$= e^{-\frac{\omega}{v}(z_2 - z_1)} |\delta\underline{\psi}(\omega)|^2,\ z_1 < z_2 \tag{23}$$

This incidates the phase of the CPSD of a propagation perturbation is linear with frequency, thus the slope of the CPSD phase angle versus frequency plot yields,

$$\text{Slope} = \frac{(z_2 - z_1)}{v} = \frac{d\theta}{d\omega}$$

In our case, $v = C_{2\phi}$, $z_2 = z_{\text{Lower}}$ and $z_1 = z_{\text{upper}}$, thus we have:

$$C_{2\phi} = \left[(z_{\text{lower}} - z_{\text{upper}})\ 360°\right] \left(\frac{d\theta}{df}\right)^{-1}, \tag{24}$$

The CPSD's were calculated using a Hewlett Packard 3562A dynamic signal analyzer. This technique proved a useful independent verification that the time-of-flight measurements accurately indicated the propagation speed. A typical phase vs. frequency plot is given in Figure 14. It can be seen to be approximately linear.

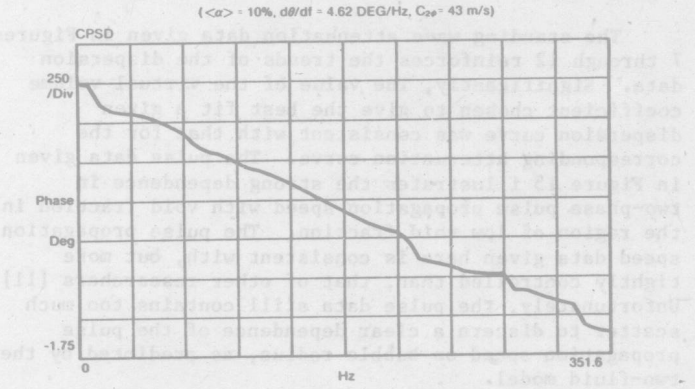

Figure 14: Phase Angle vs. Frequency for Cross-Spectrum Betwen Side Mounted Transducers C and B.

The pressure pulse propagation data taken in this study is presented in Figure 15.

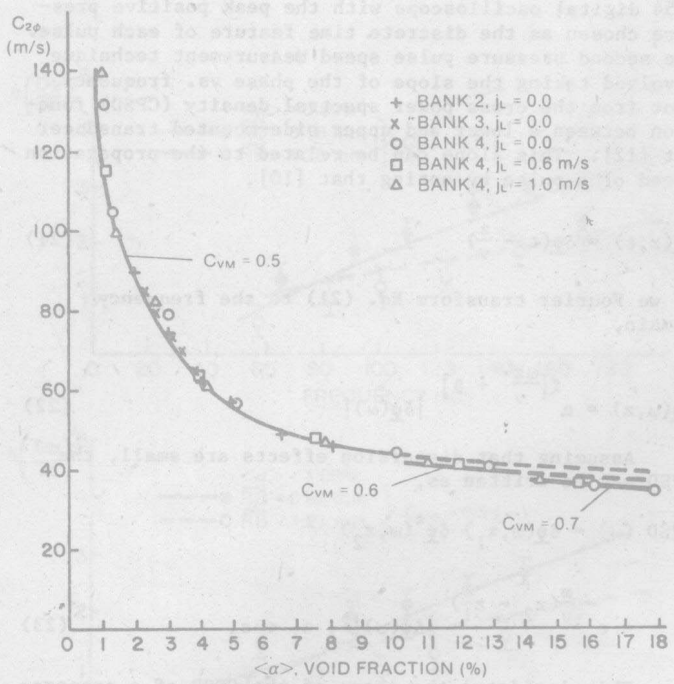

Figure 15: Pressure Pulse Propagation Speed vs. Global Void Fraction

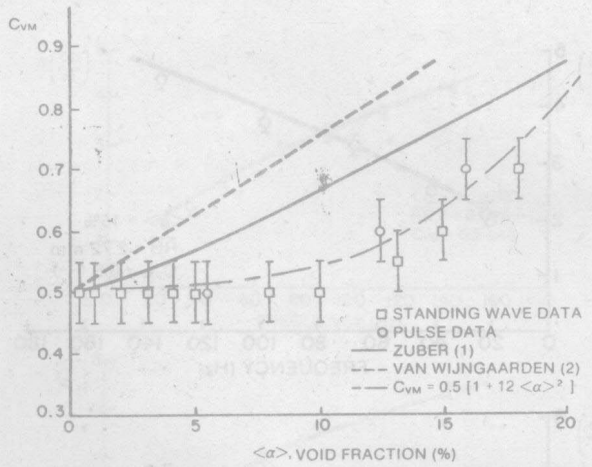

Figure 16: Virtual Mass Coefficient vs. Global Void Fraction

DISCUSSION OF RESULTS

The standing wave dispersion data given in Figure 3 clearly shows the strong dependence of the propagation speed of pressure perturbations on bubble radius. This effect is due to the dependence of the propagation speed on the interfacial heat transfer between the two phases. The larger bubbles have less interfacial area available for heat transfer and thus exhibit a more adiabatic process. It can also be noted that propagation speed decreases with frequency. More time exists for heat transfer at the lower frequencies thus promoting a more isothermal process. It is significant to note that all the standing wave measurements were taken in a frequency domain far below bubble resonance.

The standing wave attenuation data given in Figures 7 through 12 reinforces the trends of the dispersion data. Significantly, The value of the virtual volume coefficient chosen to give the best fit a given dispersion curve was consistent with that for the corresponding attenuation curve. The pulse data given in Figure 15 illustrates the strong dependence in two-phase pulse propagation speed with void fraction in the region of low void fraction. The pulse propagation speed data given here is consistent with, but more tightly controlled than, that of other researchers [11]. Unfortunately, the pulse data still contains too much scatter to discern a clear dependence of the pulse propagation speed on bubble radius, as predicted by the two-fluid model.

The measured variation of the virtual volume coefficient is given in Figure 16 for both the standing wave data and the pulse data. An empirical fit to these data is given by,

$$C_{VM} = 0.5 \left[1 + 12 \langle\alpha\rangle^2\right] \qquad (\langle\alpha\rangle < 20\%) \quad . \qquad (25)$$

It is interesting to note that the measured variation of the virtual volume coefficient with void fraction is significantly less than that predicted by the models of Zuber [2], and Van Wijngaarden [3]. The fact that the value of C_{VM_o} in Eqs. (1) & (2) was 0.50 may have caused some of this discrepancy. This choice of C_{VM_o} is only appropriate for spherical bubbles. Bubbles of radius exceeding 1.5 mm were not spherical in this experiment.

REFERENCES

1. Drew, D., Cheng, L. and Lahey, R.T., Jr., "The Analysis of Virtual Mass Effects in Two-Phase Flow", Int. Journal of Multiphase Flow, Vol. 5, 1979, pp. 233-242.

2. Zuber, N., "On the Dispersed Two-Phase Flow on the Laminar Flow Regime", Chemical Engineering Science -19 (1964) 897.

3. Van Wijngaarden, L., "Hydrodynamic Interaction" Between Gas Bubbles in Liquid", Journal of Fluid Mechanics (1976) Vol. 77, Part 1, pp. 27-44.

4. Mokeyev, Yu. G., "Effect of Particle Concentration on Their Drag and Induced Mass", Fluid Mech. Soviet Research 6 (1977) 161.

5. Henry, R.E., Grolmes, M.A. and Fauske, H.K., "Pressure Pulse Propagation in Two Phase One-and Two-Component Mixtures", ANL-7792, 1971.

6. Chernyy, I.M., and Srebnyuk, S.M., "Phase Slip in a Flow of a Gas-Liquid Mixture", Fluid Mechanics - Soviet Research, Vol. 8, No. 3, pp. 86-92, 1979.

7. Kuo, J.T., "Interphase Momentum Transfer in the Flow of Bubbles Through Nozzles", EPRI NP-980, 1979.

8. Cheng, L-Y., Drew, D.A., and Lahey, R.T., Jr., "An Analysis of Wave Dispersion, Sonic Velocity, and Critical Flow in Two-Phase Mixtures", NUREG CR/3372, July, 1983.

9. Cheng, L-Y, Drew, D.A., and Lahey, R.T., Jr., "An Analysis of Wave Propagation in Bubbly Two-Component Two-Phase Flow", Journal of Heat Transfer, Vol. 107, May, 1985, pp. 402-408.

10. Kosály, G., Albrecht, R.W., Crowe, R.D. and Dailey, D.J., "Neutronic Response to Two-Phase Flow in a Nuclear Reactor", SMORN-III, Tokyo, Japan, October 26-30, 1981.

11. Hall, P., "The Propagation of Pressure Waves and Critical Flow in Two-Phase Mixtures", Ph.D. Thesis, Heriot-Watt University, Edinburgh, G.B., 1971.

12. Bendat, J.S., Pierson, A.G., Random Data: Analysis and Measurements Procedures, Wiley-Interscience, 1971.

FLUID OSCILLATION IN PIPES CONTAINING WATER WITH UNIFORM AIR BUBBLES

T. Shioyama and K. Ohtomi
Toshiba Research and Development Center
Kawasaki-City, Kanagawa, Japan

ABSTRACT

Oscillatory pressures in a vertically standing water column, uniformly containing air bubbles, were measured. The greatest oscillatory pressure was at the oscillating frequency close to the resonant frequency altered by air mixing. The results were also compared with an analysis using a method which was typically applied to single phase fluid, but included the air bubbles effect as sonic velocity. Results showed satisfactory agreement with each other.

NOMENCLATURE

a : sonic velocity
A : area of pipe
Ap : piston area
c : oscillator acceleration
D : pipe diameter
e : pipe wall thickness
E : Young's modulus of pipe wall
f : oscillating frequency
[F]: field transfer matrix
H : oscillatory pressure head
K : water bulk modulus of elasticity
l : pipe length
m : mass of free air per unit volume of air-water mixture
p : absolute pressure
P0 : pressure measurement location (at the bottom)
P1 : pressure measurement location (at 0.624 meter from the bottom)
P2 : pressure measurement location (at 1.824 meter from the bottom)
Q : pulsatic flow rate
R : gas constant
T : absolute temperature
[V]: fluid state vector
Z : characteristic impedance ($= \frac{a}{gA}$)
g : gravitational acceleration
α : void fraction
γ : propagation constant ($\gamma^2 = -\frac{\omega^2}{a^2}$)
ω : oscillating angular frequency ($\omega = 2\pi f$)
ρ : water density

Subscripts

B : bottom of the pipes
T : top of the pipes

INTRODUCTION

It is well-known that, if periodic oscillatory fluid pressure or fluid discharge source is presumed in pipeline systems, for example, if reciprocating pumps or oscillating valves exist, the response pressure at each point in the pipeline increases quite a bit, when the oscillator frequency equals the internal fluid's resonant frequency. This resonant frequency is determined mainly by the pipeline length and the acoustic velocity of fluid. It is usually analyzed by using a transfer function procedure to predict oscillatory pressures in the fluid. This analysis method is described in the text by Wylie and Streeter [1].

Pipe vibrations caused by internal liquid were studied by e.g. Hatfield et al. [2]. However, in engineering practice, these vibrations are typically analyzed using the previous transfer function procedure about fluid and a finite element solution about piping structures.

Then, when gas bubbles exist in the pipes, the oscillating pressure field behavior differ, in comparison with the case when the liquid contains no gas. Actually, an unexpectedly large oscillatory pressure, which is presumed to be caused by the existence of air mixing, is ocassionally experienced in a pipeline, resulting in unusual pipe vibrations and noises.

It is a well-known fact that the gas content in liquids tends to reduce the propagation velocity for a pressure wave in a pipeline. Sonic velocity in liquid-gaseous two-phase flow in a pipe has been studied since the papers by Kobori et al. [3] and Silberman [4]. Henry et al. [5] measured the pressure pulse, passing two separate locations using piezoelectric transducers. Nguyen et al. [6] proposed an ideal model, considering the interface of one phase to act as an elastic wall for the other phase.

Oscillating two-phase fluid phenomena are also influenced by this reduction in sonic velocity, perhaps, as a consequence of changed resonance. However, to the author's knowledge, few papers have been reported to confirm and explain these phenomena completely. It is also presumed that the behaviors are affected by two-phase flow pattern. The present paper is concerned with fluid oscillation in a pipeline containing water with almost uniform air bubbles.

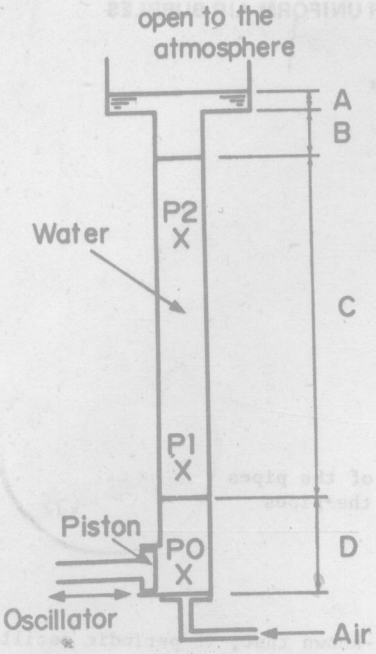

Pipe	Length	Inner Diameter	Wall Thickness	Pipe Material
	m	m	mm	
A	0.013	0.1584	3.4	Stainless Steel
B	0.300	0.0483	1.25	Stainless Steel
C	2.400	0.0485	2.0	Acrylic Resin
D	0.324	0.0483	1.25	Stainless Steel

Water density: 1000.0 kg/m^3

Water bulk modulus of elasticity
: 2.3 x 10^8 kg / m^2

Fig. 1 Test section

EXPERIMENTAL APPARATUS

Experiments were made using the test section shown in Fig. 1. The test section was made from standing pipes filled with still water, with a oscillator set up at the bottom of the pipes. The top of the pipes was open to the atmosphere. At the bottom, there was a pulsatic discharge source, which was made up with a piston connected to the oscillator. The oscillating wave form was a sinusoidal wave. The oscillating frequency could be changed continuously from 20 Hz to 180 Hz. Air was mixed through the holes at the bottom, and air bubbles dispersed uniformly rose in the water. The pipes were mostly made of transparent acrylic resin. We could justify the uniformity of void fraction with the eye or photographs.

Three strain-gauge pressure transducers were mounted at the pipe wall in order to measure dynamic pressures in water or air-water mixtures. Individual transducer locations were at the bottom (P0), at 0.624 meter (P1) and 1.824 meter (P2) from the bottom.

The water level was 3.154 meters. Void fraction was obtained by measuring the water-air mixture level. The measured void fraction error was ±0.04 %.

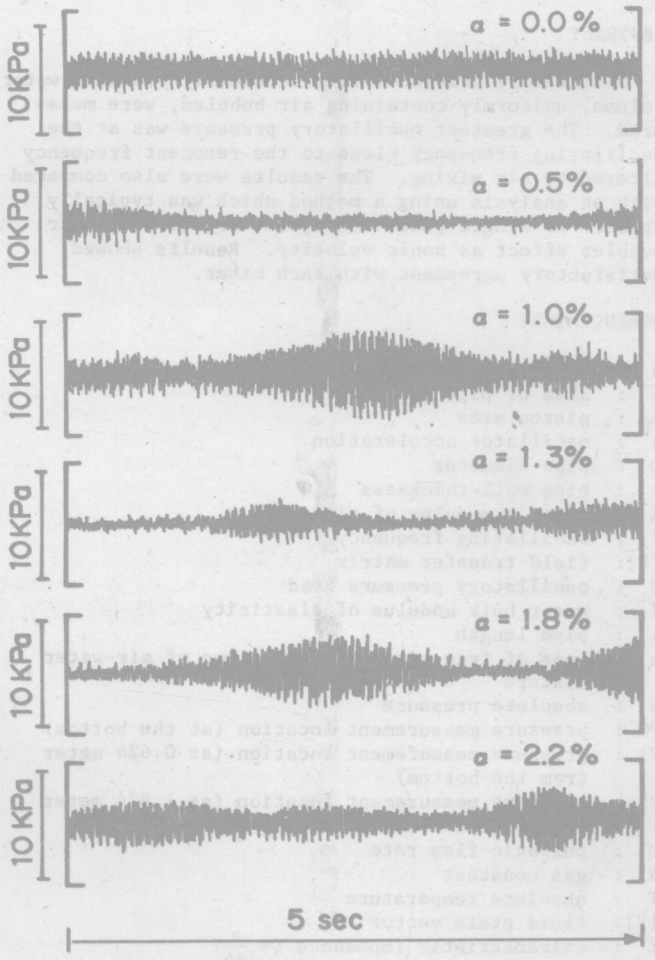

Fig. 2 Oscillatory pressure time histories (measured at P1, f = 63.4 Hz, $Q_B = 8.0 \times 10^{-5}$ m^3/sec)